YIDDISH Vol 10 Issue 04,Oct 2020
ISSN NO: 0364-4308

Eliminating the Effect of Load Variation on a Boost Converter's Predictive Current using an EKF

MUNTHA GIRIBABU[1],Y.VAMSI BABU[2],
ASSOCIATE PROFESSOR[1], ASSISTANT PROFESSOR[2],
DEPARTMENT OF EEE
PBR VISVODAYA INSTITUTE OF TECHNOLOGY AND SCIENCE::KAVALI

Abstract:

In order to achieve high resolution current regulating in a boost converter, precise measurement of the inductor current is essential. Inductor current is often measured using current sensors. Present-day sensors and their associated processing circuits, however, add substantial hardware expense, delay, and noise to the system. They are also a potential dependability risk for the system. Therefore, modern sensor less control methods may provide low-cost and dependable options for many boosts converter uses. The obtained accurate model indicates that the boost converter is a nonlinear system due to the presence of many parasitic. We suggest using an Extended Kalman Filter (EKF) to estimate the inductor current and filter the output voltage. The system may have the same benefits as the censored current control mode by using this method. In order to put EKF into action, the load value is required. However, there may be times when the workload changes. This might cause inaccurate current estimate and a distorted voltage at the filter's output. An LVEE (load variation elimination effect elimination) module is implemented to rectify this situation. To further control the current, a predictive average current controller is used. Since it only takes two switching cycles for the current to reach its reference, the transient responsiveness is considerably enhanced in comparison to traditional voltage-controlled systems. At last, experimental results are shown to prove the proposed algorithm's stable operation and output tracking capacity under large-signal transients.

Keywords:

The load fluctuation effect is removed by using a boost converter, sensor less predictive current control, an expanded Kalman filter, and a variable current source.

Introduction

Recent years have seen an uptick in interest in studying current mode digital controlled DC-DC converters [1-7]. Boost converters are among the most used DC-DC converters; hence their regulation has been the subject of much study [8-10]. Its reaction time and loop gain bandwidth are both improved over voltage mode-controlled systems. However, accurate current sensors are necessary for effective current feedback control to be realized. In [11], the author summarizes the present state of the art in sensing technology. The gigantic magnetoresistance effect based current sensor is one example of a technology for current sensing that offers a low-cost isolation solution [12,13]. However, three kinds of current sensors are often used in a boost converter. Three distinct approaches have been developed for measuring switching current: one employs a shunt resistor in series with the switching device [14,15], another utilizes a current mirror to reconstruct the switch component current [16], and the third makes use of Hall effect sensors. In addition to potential power losses, EMI issues have been reported with both types [17]. The third form is the most precise, and it is possible to make it very impervious to electromagnetic interference [18]. Most Hall current sensors, however, come at a hefty price. The current sensors and signal processing circuits increase the converter's price and add delay and noise to the control circuitry. As a result, the sensor less current controlled boost converter has significant potentials in both academic and industrial applications due to its ability to work in current control mode with all the aforementioned benefits but without a current detecting module.

Current observers are often employed to make current estimates for sensor-free current control. The effectiveness of the present observer is highly dependent on the precision with which the system is modelled [19-21]. Several methods of simulating boost converters are examined in [22–24]. The model provided by P. Madya in 2001 [25], which is based on the current observer, is fairly realistic. However, this strategy's implementation is considerably too complicated for real time digital control. In 2004, [26] proposed a simpler approach that uses a feed forward current observer depending on the input voltage, which successfully eliminates the effects of the output voltage changes on the current observer. However, the method did not take into account the impact of the parasitic parameters, therefore the present estimate error is rather high. The boost converter's dynamic responsiveness may be enhanced using a sensor less current control method developed in [27] that is based on the Control-Lyapunov Function. To get rid of the double frequency ripple, a novel sensing approach is developed that uses maximum and lowest values to determine the output voltage's mean value. This allows for a substantial boost in the voltage controller's bandwidth. Cho looked into a sensor less controller for boost converters based on a state observer and Lyapunov's direct technique [28]. To calculate the inductor current from the input and output voltages and the switch control signal, a state observer is built. In terms of transient reaction, the system performs well.

System Control Structure and Mathematical Model

The System Control Structure

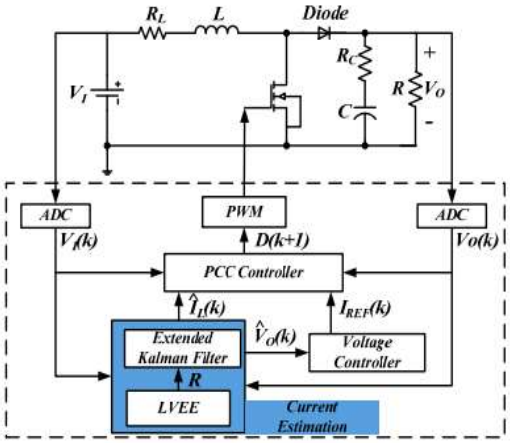

Figure 1. Control diagram of an EKF based sensor less current controlled boot converter.

Figure 1 depicts the construction of a boost converter using the suggested technique. Two control loops make up the system. The EKF is a filter that is part of the outer loop, which is a voltage control loop that uses a PI controller to manage the output voltage () V k O. Its results are now used as the standard. A current estimate module and a PCC controller make up the inner loop's current control system. This article explores the whole procedure for designing current loops. The present estimating component is a hybrid between an EKF and LVEE. The EKF allows for accurate estimate of the typical inductor current and noise-free measurement of the output voltage. The LVEE gets rid of fluctuating loads completely. The average current control mode is used to regulate the flow of current. Based on the input and output voltage samples, the PWM duty ratio for the next switching cycle may be calculated. If this is done, the discrepancy between the ideal and real average currents may be fixed.

Proper Mathematical Representation of the Boost Converter

An accurate model of the system is required since the performance of the present estimate is dependent on the correctness of the model. In order to accurately represent a boost converter, we construct a set of parasitic parameters. The boost converter's analogous model (shown in Figure 2) includes a number of parasitic parameters. RL is the inductor's parasitic resistance, RDS is the MOSFET's switching on resistance, RD is the diode's conduction resistance, VD is the diode's forward voltage drop, and RC is the capacitor's equivalent series resistance (ESR).

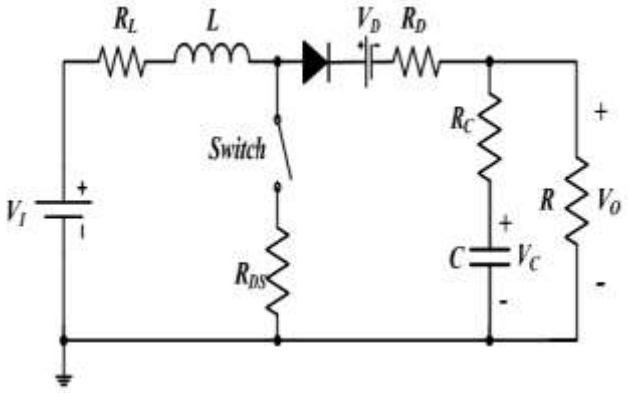

Figure 2. The accurate model of a boost converter with a number of parasitic parameters.

Setting inductor current IL(t) and capacitor voltage VC(t) as the state variables, the system state function is derived as follows. When the switch is on, the capacitor is discharged to supply energy to load, then

$$V_O(t) = V_C(t) - \frac{V_O(t)}{R} R_C$$

Equally as Equation (1)

$$V_O(t) = \frac{R}{R + R_C} V_C(t)$$

During switching on period, discharging current of capacitor is −VO(t)/R, the system state function is

$$L\frac{dI_L(t)}{dt} = V_I - I_L(t)(R_L + R_{DS})$$
$$C\frac{dV_C(t)}{dt} = -\frac{V_C(t)}{R + R_C}$$

When the switch is off, the inductor charges capacitor and provides energy for load

$$V_O(t) = V_C(t) + \left[I_L(t) - \frac{V_O(t)}{R} \right] R_C$$

Equally as Equation (4)

$$V_O(t) = \frac{R}{R + R_C} \left[V_C(t) + I_L(t) R_C \right]$$

During the switching off period, charging current of capacitor is IL(t) − VO(t)/R, the system state function is

$$L\frac{dI_L(t)}{dt} = V_I - V_D - \left(R_L + R_D + \frac{RR_C}{R + R_C} \right) I_L(t) - \frac{R}{R + R_C} V_C(t)$$
$$C\frac{dV_C(t)}{dt} = \frac{R}{R + R_C} I_L(t) - \frac{V_C(t)}{R + R_C}$$

Setting

$$X(t) = [X_1(t) \quad X_2(t)]^T = [I_L(t) \quad V_C(t)]^T,$$

Equations (3) and (6) can be presented as

Switching on: $\dot{X}(t) = F_1 X(t) + G_1$

Switching off: $\dot{X}(t) = F_2 X(t) + G_2$

where F1, G1, F2 and G2 are

$$F_1=\begin{bmatrix}-\frac{R_L+R_{DS}}{L} & 0\\ 0 & -\frac{1}{C(R+R_C)}\end{bmatrix}\quad G_1=\begin{bmatrix}\frac{V_I}{L}\\ 0\end{bmatrix}$$

$$F_2=\begin{bmatrix}-\frac{RR_C+(R+R_C)(R_L+R_D)}{L(R+R_C)} & -\frac{R}{L(R+R_C)}\\ \frac{R}{C(R+R_C)} & -\frac{1}{C(R+R_C)}\end{bmatrix}\quad G_2=\begin{bmatrix}\frac{V_I-V_D}{L}\\ 0\end{bmatrix}$$

At first, integrate Equations (7) and (8), respectively, during switching on 0 ~ dT and switching off dT ~ T periods, then add them together and divide the sum by switching period T, the average state function during the whole switching cycle is obtained as Equation (11)

$$\dot{X}(t)=\left[F_2+(F_1-F_2)d(t)\right]X(t)+(G_1-G_2)d(t)+G_2$$

According to capacitor charging balance principle, when the system is in steady state, average output voltage VO is equal to average capacitor voltage VC. So, X(t) can be described as

$$X(t)=[I_L(t)\quad V_O(t)]^T$$

Equation (11) reveals that the boost converter is a nonlinear system due to the presence of the nonlinear item X(t)d(t). Since nonlinear systems only employ the EKF, it is natural to employ it for current estimates and the output voltage filter.

Methodology for Making Future Predictions

First, an EKF is presented in this section for sensor less current control of boost converters. Then, an LVEE approach is researched. In addition, the steady-state error elimination of the filtered output voltage is analysed theoretically by use of the LVEE module.

An Estimation Kalman Filter

In Section 2, a detailed model of a boost converter is developed. This allows us to derive the EKF used in current estimates and the voltage filter. It is necessary to discretize the boost converter's state function before implementing the EKF-based digital control. When Equation (11) is discretized, it becomes the boost converter's nonlinear random differential function.

$$\begin{aligned}X(k)&=AX(k-1)+BX(k-1)d(k)+Cd(k)+D+w(k-1)\\&=f\left[X(k-1),d(k),w(k-1)\right]\end{aligned}$$

Measurement function is

$$Z(k)=HX(k)+v(k)$$

w here, the input is duty ratio d(k), Z(k) is the measurement variable, which is the output voltage; VO(k), w(k − 1) and v(k) are noises of the process and measurement. They are not coupled. A, B, C and D in discrete domain can be described as

$$A=I+TF_2,\ B=T(F_1-F_2),\ C=T(G_1-G_2),\ \text{and}\ D=TG_2.\ H$$

H is the observation matrix in discrete domain and H = [1 0]. Essentially, an EKF consists of a group of mathematical functions to realize prediction, adjusts and estimation. By using EKF, the covariance of estimation error can be reduced as low as possible. According to Equation (12), the updating functions of EKF are

$$\tilde{X}(k) = A\hat{X}(k-1) + B\hat{X}(k-1)d(k) + Cd(k) + D$$

$$\tilde{P}(k) = A(k)P(k-1)A^T(k) + Q$$

Equations (14) and (15) are the state and covariance prediction equations. Q is a covariance. The state and covariance of current switching cycle can be derived from last switching cycle. Where X k( ) % is the previous state estimation of the kth cycle, while ˆ X k(1) − is the post state estimation of the (k − 1)the cycle. P k( ) % is the previous estimation covariance of the kth cycle, and P(k − 1) is the post estimation covariance of the (k − 1)the cycle. A(k) is a Jacob matrix of the process and it can be derived from Equation (16).

$$A(k) = \frac{\partial f\left[X(k-1), d(k)\right]}{\partial X(k-1)} = A + Bd(k)$$

Using measurements to correct the previous state and covariance of estimation errors, then the measurement update matrix of EKF is

$$Kg(k) = \tilde{P}(k)H^T\left[H\tilde{P}(k)H^T + R\right]^{-1}$$

$$\hat{X}(k) = \tilde{X}(k) + Kg(k)\left[Z(k) - H\tilde{X}(k)\right]$$

$$P(k) = [I - Kg(k)H]\tilde{P}(k)$$

Equations (17)–(19) are the correction equations for state and covariance predictions. Kg(k) is the filter gain. R is a covariance. All the equations of the EKF are presented from Equations (14) to (19). As above process shows, only input and output voltages need to be sampled. Then the inductor current can be estimated and the output voltage can be filtered.

Average Current Control Based on PCC

In this paper, a leading edge PWM modulation scheme is used. According to [31], sub harmonic oscillation exists in average control mode. Because when the average current equals to reference current in steady state, the peak current may not be a constant value and this causes the oscillation. In this section, a novel PCC based control algorithm is proposed. When any disturbance happens in current control loop, the current controller regulates the peak current to constant at first, and then the average current is also regulated to reference value in the following switching cycles. Figure 3 shows the inductor current waveform under proposed average current control mode by using the leading edge PWM modulation method .

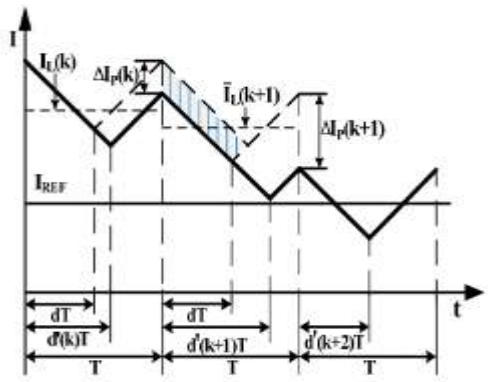

Figure 3. Inductor current waveform under proposed average current control mode.

Assuming there is a disturbance on inductor peak current in the kth switching cycle, and it is described as Equation (32).

$$\Delta I_P(k) = \left[M_1(k) + M_2(k) \right] \Delta d(k) T$$

Where

$$\Delta d(k) = d - d(k),$$

d is the duty ratio of steady state, and it can be expressed as

$$\Delta I_P(k) = \left[M_1(k) + M_2(k) \right] \Delta d(k) T$$

M1(k) is the positive slope of inductor current in the kth switching cycle, and M2(k) is the negative slope absolute value. They are described as Equations (33) and (34).

$$M_1(k) = \frac{V_I(k) - I_{AV}(k)(R_L + R_{DS})}{L}$$

$$M_2(k) = \frac{V_O(k) - V_I(k) + V_D + I_{AV}(k)(R_L + R_D + R_{COMP})}{L}$$

where RCOMP = RC + d'd/2fC, f is the switching frequency. In Figure 3, the shade area is the difference required to maintain the (k + 1)the cycle peak current stays the same as the kth cycle and it can be derived as

Experimental Results In order to verify the proposed algorithm, a series of experiments in steady state and transient state with load and line voltage changing conditions are carried out for a boost converter. For comparison the same experiments are implemented by using conventional voltage control mode with the same hardware. Design parameters of the target boost converter are shown in Table 1.

Table 1. Specifications of the tested boost converter.

Input voltage	6 V
Output voltage	12 V
Rated output current (ROC)	0.5 A
Voltage ripple under ROC	1%
Switching frequency	50 kHz

The constructed boost converter has both a control and a power module. A Texas Instruments TMS320F2812 DSP forms the brains of the controller. Input and output voltages are sampled at the start of each switching cycle by the power section, which also contains the primary power stage and signal sampling circuits. Infineon BSZ110N06NS3 MOSFET is the power stage's switching device; Panasonic EEHZC1E101XP is the output capacitor; and Liteon SB350 is the diode. Table 2 lists the details of the individual parts. A 12-bit DAC TVL5616 is used to simultaneously output the calculated average current for monitoring. The real current through the inductor is read off by a current probe with a 200 mV/A precision. The DAC output is normalized for straightforward evaluation. Channel 1 uses AC mode sampling with high resolution to clearly display voltage ripple, while Channel 2 displays the output voltage itself at a resolution of 2 v/div. Channel 2 represents an estimated average current waveform, whereas Channel 1 displays the actual current waveform, denoted by the symbol il.

Table 2. Specifications of hardware platform\

Inductance of the power inductor	120 µH
Inductor winding resistance	250 mΩ
Capacitance of the output capacitor	75 µF
ESR value of the output capacitor	50 mΩ
MOSFET R_{DS}	11 mΩ
Diode forward Voltage	0.7 V
Diode forward resistance	100 mΩ

Experiments for the LVEE module function verification

Voltage and current waveforms at steady state without the LVEE module are shown in Figure 4a,b. Figure 4a shows the steady-state output voltage to be 11.57 V, with a maximum steady-state inaccuracy of 0.43 V. Current estimation steady state error of 0.13 A is seen in Figure 4b, where the estimated average current is 1.03 A whereas the real average current should be 1.16 A.

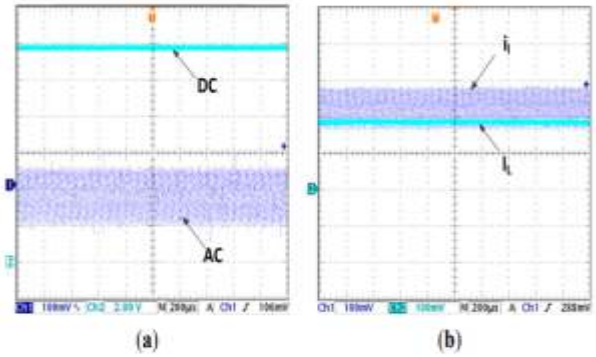

Figure 4. (a) Steady state output voltage without using LVEE module; (b) Steady state inductor current without using LVEE Module When the LVEE module is added, the steady state output voltage and current waveforms are presented in Figure 5a,b. Neither the output voltage nor the estimated average current has steady state error.

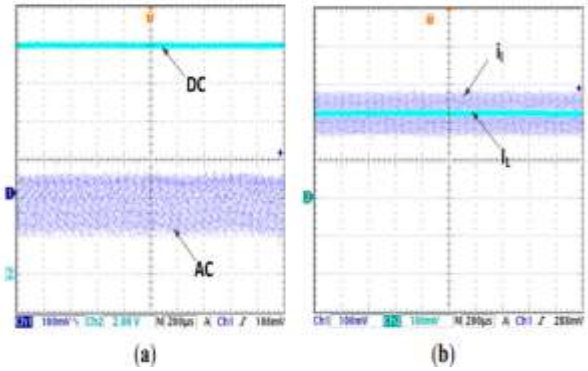

figure 5. (a) Steady state output voltage by using LVEE module; (b) Steady state inductor current by using LVEE Module.

Conclusions

A detailed mathematical model of a boost converter is constructed in this study, complete with a variety of parasitic factors. Using an EKF current observer and LVEE module, we are able to estimate current for sensor less control of the boost converter. By doing a thorough investigation of the LVEE module, we are able to better understand how and why it may rectify the output voltage steady state mistake. PCC is used for current regulation, and it is based on the average current mode. In two transitions, the current may approach the nominal value. Using all of these methods, the system achieves impressive results in terms of both current estimate and dynamic responsiveness. In addition, the LVEE module may be used to get rid of the steady-state inaccuracy in the output voltage under load-variation situations. All of these assertions are supported by experiments.

References

[1]. Min, R.; Chen, C.; Zhang, X.D.; Zou, X.C.; Tong, Q.L.; Zhang, Q. An Optimal Current Observer for Predictive Current Controller Buck DC-DC Converters. Sensors 2014, 14, 8851–8868.

[2]. Veerachary, M.; Saxena, A.R. Design of Robust Digital Stabilizing Controller for Fourth-Order Boost DC–DC Converter: A Quantitative Feedback Theory Approach. IEEE Trans. Ind. Electron. 2012, 59, 952–963.

[3]. Kelly, A.; Rinne, K. Sensor less current-mode control of a digital deadbeat DC–DC converter. In Proceedings of the 19th Annual IEEE APEC, Anaheim, CA, USA, 22–26 February 2004; pp. 1790–1795.

[4]. Choi, B.; Lim, W.; Choi, S.; Sun, J. Comparative Performance Evaluation of Current-Mode Control Schemes Adapted to Asymmetrically Driven Bridge-Type Pulse width Modulated DC-to-DC Converters. IEEE Trans. Ind. Electron. 2008, 55, 2033–2042.

[5]. Qin, M.; Xu, J. Improved Pulse Regulation Control Technique for Switching DC–DC Converters Operating in DCM. IEEE Trans. Ind. Electron. 2012, 60, 1819–1830.

[6]. Saggini, S.; Stefanutti, W.; Tedeschi, E.; Mattavelli, P. Digital deadbeat control tuning for DC–DC converters using error correlation. IEEE Trans. Power Electron. 2007, 22, 1566–1570.

[7]. Zhang, F.; Xu, P.J. A Novel PCCM Boost PFC Converter with Fast Dynamic Response. IEEE Trans. Ind. Electron. 2011, 58, 4207–4216.

[8]. Taeed, F.; Salam, Z.; Ayob, S.M. FPGA Implementation of a Single-Input Fuzzy Logic Controller for Boost Converter with the Absence of an External Analog-to-Digital Converter. IEEE Trans. Ind. Electron. 2012, 59, 1208–1217.

[9]. Zhang, Q.; Min, R.; Tong, Q.L.; Zou, X.C.; Liu, Z.L.; Shen, A.W. Sensorless Predictive Current Controller DC–DC Converter With a Self-Correction Differential Current Observer. IEEE Trans. Ind. Electron. 2014, 61, 6747–6757.

[10]. Trescases, O.; Parayandeh, A.; Prodi'c, A.; Ng, W.T. Sensorless digital peak current controller for low-power DC–DC SMPS based on a bi-directional delay line. In Proceedings of the IEEE Power Electronics Specialists Conference, Jeju, Korea, 17–21 June 2006; pp. 1670–1676.

[11]. Ziegler, S.; Woodward, R.C.; Iu, H.; Borle, L.J. Current sensing techniques: A review. Sensors 2009, 9, 354–376.

[12]. Ouyang, Y.; He, J.; Hu, J.; Wang, S.X. A current sensor based on the giant magnetoresistance effect: Design and potential smart grid applications. Sensors 2012, 12, 15520–15541.

[13]. Jantaratana, P.; Sirisathitkul, C. Low-cost sensors based on the GMI effect in recycled transformer cores. Sensors 2008, 8, 1575–1584.

[14]. Aiello, O.; Fiori, F. A new mirroring circuit for power MOS current sensing highly immune to EMI. Sensors 2013, 13, 1856–1871.

[15]. Sachin, R.; Qadeer, K.; Sarvesh, B.; Damian, S.; Arun, R.; Willian, M.; Pavan, K.H. A 1.2-A buck-boost LED driver with on-chip error averaged senseFET-based current sensing technique. IEEE J. Solid-State Circuits 2011, 46, 2772–2783.

[16]. Milanés-Montero, M.I.; Gallardo-Lozano, J.; Romero-Cadaval, E.; González-Romera, E. Hall-effect based semi-fast AC on-board charging equipment for electric vehicles. Sensors 2011, 11, 9313–9326.

[17]. Aiello, O.; Grovetti, P.; Fiori, F. Investigation on the susceptibility of hall-effect current sensors to EMI. In Proceedings of the EMC Europe 2011, York, UK, 26–30 September 2011; pp. 368–372.

[18]. Aiello, O.; Fiori, F. A New MagFET-Based integrated current sensor highly immune to EMI. Microelectron. Reliab. 2013, 53, 573–581.

[19]. Yang, P.; Xu, J.; Zhou, G.; Zhang, F. Analysis of sensorless peak current mode controlled quadratic boost converter. In Proceedings of the ISIE, Hangzhou, China, 28–31 May 2012; pp. 200–204.

[20]. Qahouq, J.A.A.; Arikatla, V.P. Power converter with digital sensorless adaptive voltage positioning control scheme. IEEE Trans. Ind. Electron. 2011, 58, 4105–4116.